Mach Stability Improvements Using an Existing Second Throat Capability at the National Transonic Facility (Invited)

David T. Chan*, Sundareswara Balakrishna†, Eric L. Walker‡, and Scott L. Goodliff§
NASA Langley Research Center, Hampton, VA, 23681

Recent data quality improvements at the National Transonic Facility have an intended goal of reducing the Mach number variation in a data point to within ± 0.0005, with the ultimate goal of reducing the data repeatability of the drag coefficient for full-span subsonic transport models at transonic speeds to within half a drag count. This paper will discuss the Mach stability improvements achieved through the use of an existing second throat capability at the NTF to create a minimum area at the end of the test section. These improvements were demonstrated using both the NASA Common Research Model and the NTF Pathfinder-I model in recent experiments. Sonic conditions at the throat were verified using sidewall static pressure data. The Mach variation levels from both experiments in the baseline tunnel configuration and the choked tunnel configuration will be presented and the correlation between Mach number and drag will also be examined. Finally, a brief discussion is given on the consequences of using the second throat in its location at the end of the test section.

Nomenclature

Symbols

A_*	Minimum cross-sectional area, ft^2
A_{max}	Maximum frontal cross-sectional area of test article, ft^2
A_{TS}	Test section cross-sectional area, ft^2
$\mathcal{AR}$	Aspect ratio
AF	Axial Force, lbf
b	Wing span, in
$\bar{c}$	Mean aerodynamic chord, in
C_D	Drag coefficient, stability axis
C_{D_0}	Profile or minimum drag coefficient, stability axis
$\mathbb{C}$	Centerline
C_L	Lift coefficient, stability axis
L/D	Lift-to-drag ratio, stability axis
M_∞	Freestream Mach number
M_{local}	Local Mach number
NF	Normal force, lbf
p_s	Tunnel reference static pressure, psia
p_t	Tunnel stagnation pressure, psia
q_∞	Freestream dynamic pressure, psf
$R(\,)$	Range, max $-$ min, of a dataset
Re	Reynolds number based on mean aerodynamic chord, 10^6
S_{ref}	Wing reference area, ft^2
SF	Side force, lbf
T_t	Tunnel stagnation temperature, °F
α	Angle of Attack, deg
γ	Ratio of specific heats
ρ	Pearson correlation coefficient
ε	Total blockage factor
ε_{SB}	Solid blockage factor
ε_{WB}	Wake blockage factor

Superscripts

$'$	Fluctuating component

Units

°, deg	degrees
°F	degrees Fahrenheit
atm	atmospheres
cm	centimeter

*Research Aerospace Engineer. Configuration Aerodynamics Branch. Mail Stop 499. Member AIAA.
†Research Engineer. Vigyan, Inc. Mail Stop 274. Senior Member AIAA.
‡Research Aerospace Engineer. Configuration Aerodynamics Branch. Mail Stop 267. Senior Member AIAA.
§Test Engineer. Jacobs Technology, Inc. Mail Stop 267. Member AIAA.

ft	feet
ft^2	square feet
HP	horsepower
Hz	Hertz
in	inches
in^2	square inches
in-lbf	inch-pound force
lbf	pounds force
m	meter
psf	pounds per square foot
psia	pounds per square inch absolute
psid	pounds per square inch differential
RPM	revolutions per minute
sec	seconds

Acronyms

AIAA	American Institute of Aeronautics and Astronautics
AOA	Angle of attack
CFD	Computational Fluid Dynamics
CRM	Common Research Model
DAS	Data Acquisition System
DDAS	Dynamic Data Acquisition System
DPW	Drag Prediction Workshop
FIDO	Facility Improvements and Data Optimization
LaRC	Langley Research Center
LFC	Laminar Flow Control
MMS	Mach Measurement System
NASA	National Aeronautics and Space Administration
NTF	National Transonic Facility
ONERA	Office National d'Etudes et Recherches Aérospatiales
PF-I	Pathfinder-I
SLATE	Software for Laboratory and Automated Test Environments
STARBUKS	Subsonic Transonic Applied Refinements By Using Key Strategies
STARCS	Sjöland & Thyselius Aerodynamic Research Centre AB
T.S.	Tunnel Station
WT	Wind Tunnel

I. Introduction

Recent modifications[1] at NASA Langley Research Center's National Transonic Facility (NTF) shown in Figure 1 have focused on improving overall data quality. One of the efforts is concentrated on improving the Mach stability and reducing the pressure fluctuations in the test section, with a desired Mach number variation of $M_\infty \pm 0.0005$ as a result of the improvements . However, the ultimate goal is to improve the data repeatability of the drag coefficient C_D for full-span subsonic transport models at transonic speeds to within half a drag count ($C_D \pm 0.00005$).

The approach to achieving these goals is three-fold:

1. Investigate physics-based changes to tunnel operations such as the use of a sonic throat or the passive use of vortex generators in the high-speed diffuser.

2. Investigate software techniques such as conditional sampling and long period averaging to improve data quality.

3. Investigate facility Mach number controller upgrades and improvements to gain faster response time to within tighter tolerances.

Figure 1. Aerial photograph of the NTF.

The last two topics will not be discussed here, but are important pieces to the overall data quality improvement effort. The focus of this paper is on the use of an existing second throat capability at the NTF to create a choked condition at the end of the test section to reduce the forward propagation of downstream flow disturbances, and thereby improving the Mach number stability in the test section. The use of second throats in other transonic wind tunnels is first examined to gain perspective on this well-known technique. The Mach stability improvements at the NTF were demonstrated using both the NASA Common Research Model (CRM) and the NTF Pathfinder-I (PF-I) model in recent experiments. Sidewall static pressure data are used to verify that sonic conditions at the throat are achieved. Results will be presented showing the Mach variation levels in both the baseline tunnel configuration and the choked tunnel configuration for both models as a function of angle of attack and Mach number. Results will also be presented showing the correlation between Mach number and balance axial force for the CRM model. Finally, a brief discussion on the consequences of using the second throat in its location at the end of the section is given, focusing on

model dynamics and tunnel calibration changes. A companion paper (Ref. 2) presents a detailed discussion of the high and low frequency components of the unsteady pressure characteristics of the NTF in the baseline tunnel configuration and in the choked tunnel configuration.

A. Motivation

Future civil subsonic transport aircraft designs and research are aimed at improving aerodynamic efficiency and reducing environmental impacts.[3] The aerodynamic efficiency is expressed by the lift-to-drag ratio (L/D) and increases to this ratio can be achieved through reductions in drag. Since the majority of a subsonic commercial transports' flight profile is in the cruise portion, a reduction in the cruise drag can lead to a decrease in the airplane gross weight and thereby a reduction in its fuel consumption. As subsonic transport aircraft designs have improved with time, it is more difficult to realize cruise drag reductions, even on the order of a few drag counts.

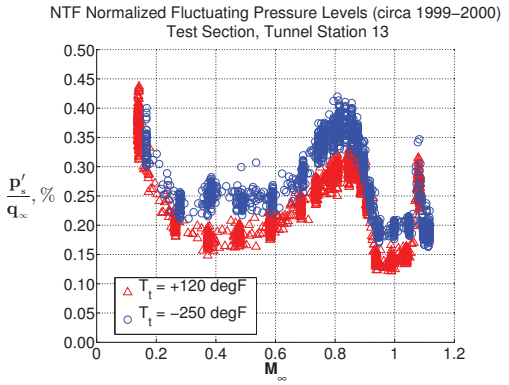

Figure 2. Normalized fluctuating pressure ratios in the NTF test section as a function of Mach number.

Data repeatability on the drag coefficient C_D of a subsonic commercial transport tested in the NTF in the early 1990's was shown to lie within a drag count ($C_D \pm 0.0001$).[4] However, over the years, research efforts on advanced subsonic transport designs have shown that data repeatability to within one drag count may not be sufficient.[5,6] It is desired that data repeatability for C_D to be within 0.5 drag count ($C_D \pm 0.00005$) or better.

Data analysis has shown that a correlation may exist between Mach number and drag coefficient variability for some models in the NTF. Consequently, it is hypothesized that if Mach variability can be reduced, drag repeatability will also improve. Although the Mach number control at NTF has historically and consistently fallen within the quoted design threshold of $M_\infty \pm 0.001$, the Mach number variability in the cruise Mach number range for commercial transports ($M_\infty \geq 0.8$) has been a concern at NTF for a number of years. Some of the variability is due to the fluctuating pressure levels in the test section reaching a maximum at around $M_\infty = 0.8$ as shown in Figure 2 and the results have been reproduced in various experiments over the years.[7,8] The use of a second throat can help to reduce the fluctuating pressure levels in the test section by reducing the amount of noise propagation from downstream sources.

B. Use of Second Throats in Transonic Wind Tunnels

Second or sonic throats in transonic tunnels are effective devices for preventing the upstream propagation of facility-generated acoustic disturbances from downstream sources such as the high-speed diffuser and liquid nitrogen injectors. Transonic tunnels that possess second throats, use them for this benefit and can also use them for fine Mach number control during model traverses. By employing the second throat at transonic Mach numbers, the fluctuating pressure levels in the test section can be significantly reduced, which in turn leads to improved Mach number stability in the test section.

Figure 3 shows four example transonic wind tunnels that possess and employ second throats during transonic operation. The main tunnel layout and a close-up view of the test section and the second throat (circled for clarity) are shown for each tunnel. The ONERA T2 cryogenic induction tunnel[9,10] in France was an injector-driven pressurized cryogenic tunnel with a 40 cm x 40 cm test section that could reach total pressures up to 5 atm, Mach numbers up to 1.1, temperatures down to -270°F, and run times between 30 to 60 seconds. The STARCS T1500 transonic wind tunnel[11,12] in Sweden is an injector-driven pressurized tunnel with a 1.5 m x 1.5 m slotted wall test section that can reach total pressures up to 5.4 atm, Mach numbers up to 1.7, and run times between 40 to 170 seconds. The European Transonic Windtunnel[13,14] (ETW) in Germany is a high Reynolds number, fan-driven, continuous-flow pressurized cryogenic tunnel with a 2.0 m x 2.4 m slotted wall test section that can reach total pressures up to 4.5 atm, Mach numbers up to 1.35, and temperatures down to -261°F. The NASA LaRC 8-foot Transonic Pressure Tunnel[15] was a fan-driven, continuous-flow pressurized tunnel with a 7.1 ft x 7.1 ft test section that could reach total pressures up to 2 atm and Mach numbers up to 1.2. The second throat was installed during the NASA Langley Laminar-Flow-Control (LFC) airfoil experiments[16,17] in the late 1980's and early 1990's.

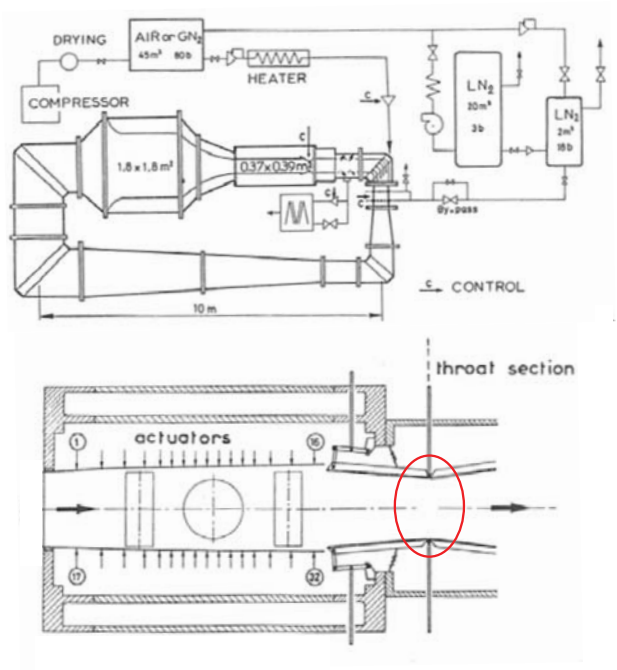

(a) ONERA T2 Cryogenic Induction Tunnel (France)

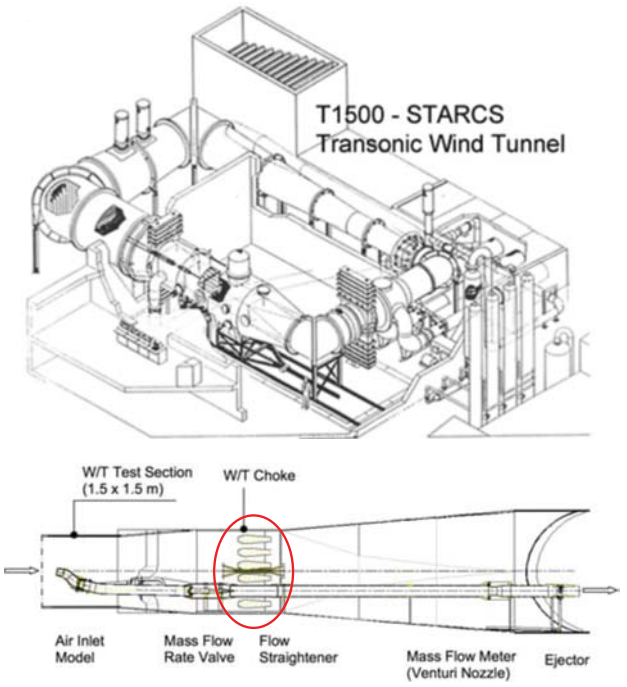

(b) STARCS T1500 Transonic Wind Tunnel (Sweden)

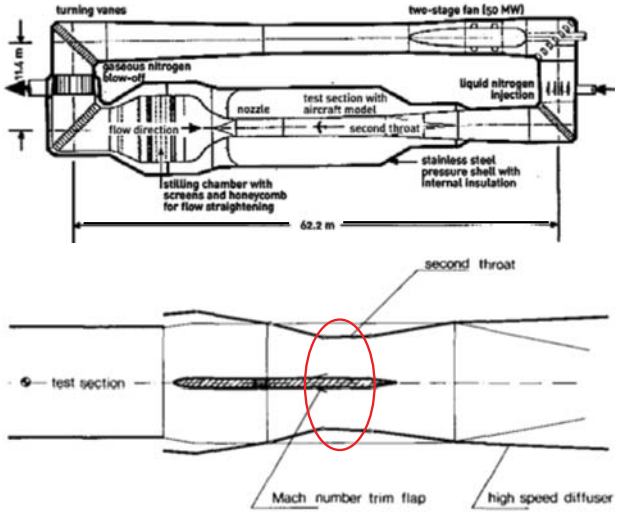

(c) European Transonic Windtunnel (Germany)

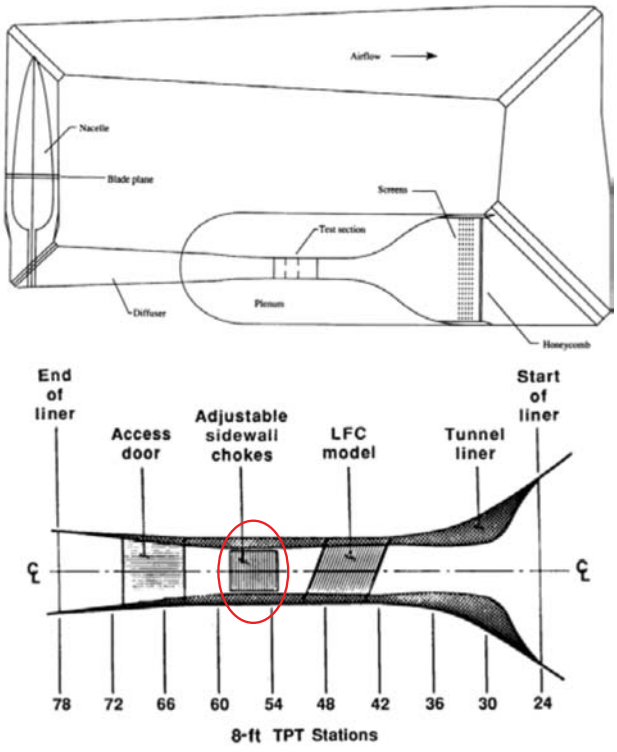

(d) NASA Langley 8-foot Transonic Pressure Tunnel (USA)

Figure 3. Examples of transonic wind tunnels (past and present) which employ second throats.

II. Wind Tunnel Description

The NTF[18] is one of a limited number of wind tunnel facilities that can achieve flight Reynolds numbers and Mach numbers for transport type aircraft for both cruise and high lift operations.[19] The tunnel is a fan-driven, closed-circuit, continuous-flow, pressurized wind tunnel capable of operating either in dry air at warm temperatures up to 120°F or in nitrogen gas from warm to cryogenic temperatures down to -270°F. The wind tunnel is capable of an absolute pressure range from 1 atmosphere to 8.3 atmospheres, a stagnation temperature range from -270°F to 120°F, a Mach number range from 0.1 to 1.2, and a maximum Reynolds number of 146x10^6 per foot at Mach 1.

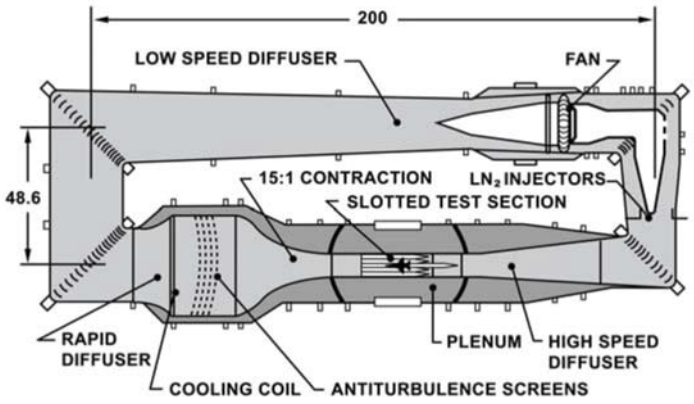

Figure 4. Major components of the NTF tunnel circuit. Linear dimensions in feet.

Figure 4 shows the major components of the NTF tunnel circuit. The NTF test section is 8.2 feet by 8.2 feet in cross section and 25 feet in length. The test section floor and ceiling are slotted (6 percent open), and the sidewalls are solid. The nominal setting for the test section walls is 0° and the nominal setting for the re-entry flaps is also 0°. The nominal setting for the model support walls downstream of the test section is a slightly divergent setting of 1.76°.

The tunnel drive system is powered by a variable-speed 135,000 HP motor that can achieve up to 600 RPM. The compressor consists of a fixed-pitch, single-stage, 25-blade fan with variable-pitch, inlet-guide vanes. To maintain rapid-response, fine Mach number control, the inlet guide vanes are varied to achieve the required compression ratio. Mach numbers are maintained to $M_\infty \pm 0.001$ or better.[20]

A. Existing Second Throat Capability

Typically, if a transonic wind tunnel possesses a second throat, it is located between the end of the test section and the beginning of the high-speed diffuser, usually just downstream of the model support structure such as an arc sector. This is done to keep the shock that is produced at the sonic throat as far downstream of the model as possible, while still allowing for a minimum area to be achieved. The NTF does not possess a second throat downstream of the arc sector, however, it does have an existing capability to set up a second throat or minimum area at the exit of the test section at station 25 feet. While this location is not ideal, it is still effective as a second throat to reduce flow disturbances propagating upstream into the test section from the high-speed diffuser and liquid nitrogen injectors.

For the series of experiments described in this paper, a combination of re-entry flaps and movable model support walls were used to create the second throat or minimum area. The re-entry flaps are typically used to optimize the mixing of the flow from the plenum and test section boundary layers into the high-speed diffuser and it was important to maintain the initial re-entry capture area when the second throat was engaged. Figure 5 highlights a typical baseline and choked tunnel configuration for a full-span model in the NTF using the re-entry flaps and model support walls. The walls were positioned by using the one-dimensional isentropic area ratio equation as shown in Equation 1 to estimate the geometric minimum area needed. However, to determine the effective minimum area and account for the wall boundary layers, the model support walls were moved incrementally from the geometric minimum settings in a trial and error method until the correct setting was determined to achieve the desired choke.

$$\frac{A_{TS}}{A_*} = \frac{\left[\frac{2}{\gamma+1}\left(1+\frac{\gamma-1}{2}M_\infty^2\right)\right]^{\left(\frac{\gamma+1}{2(\gamma-1)}\right)}}{M_\infty} \tag{1}$$

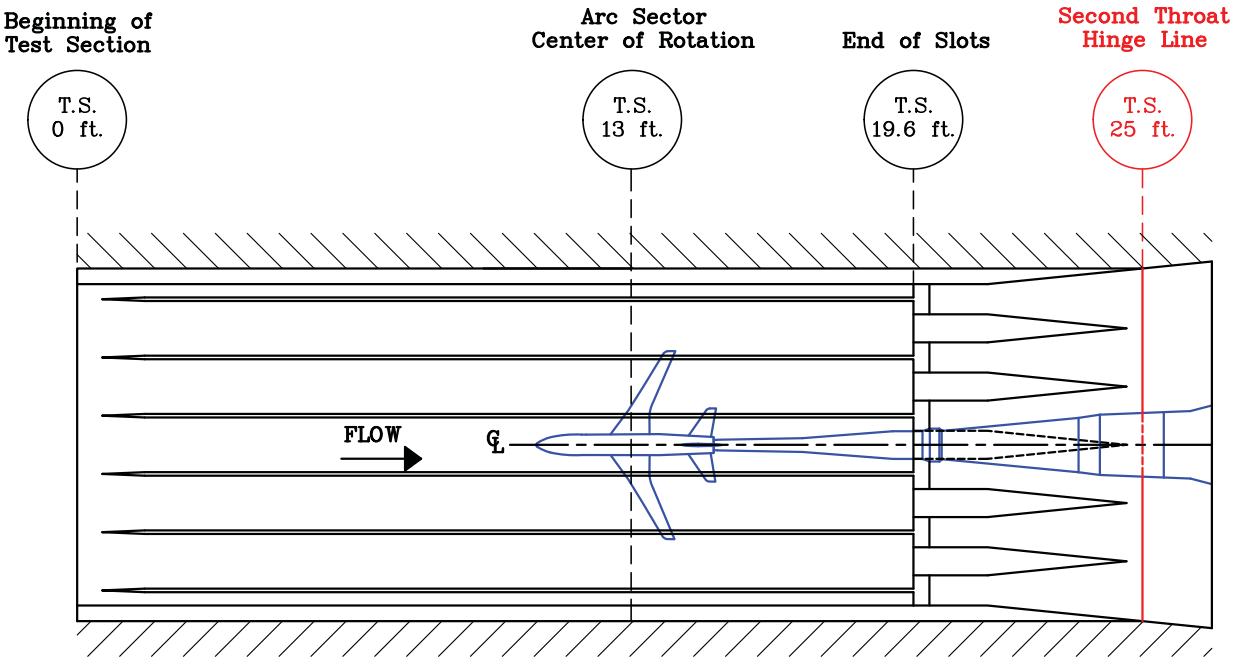

(a) Top View

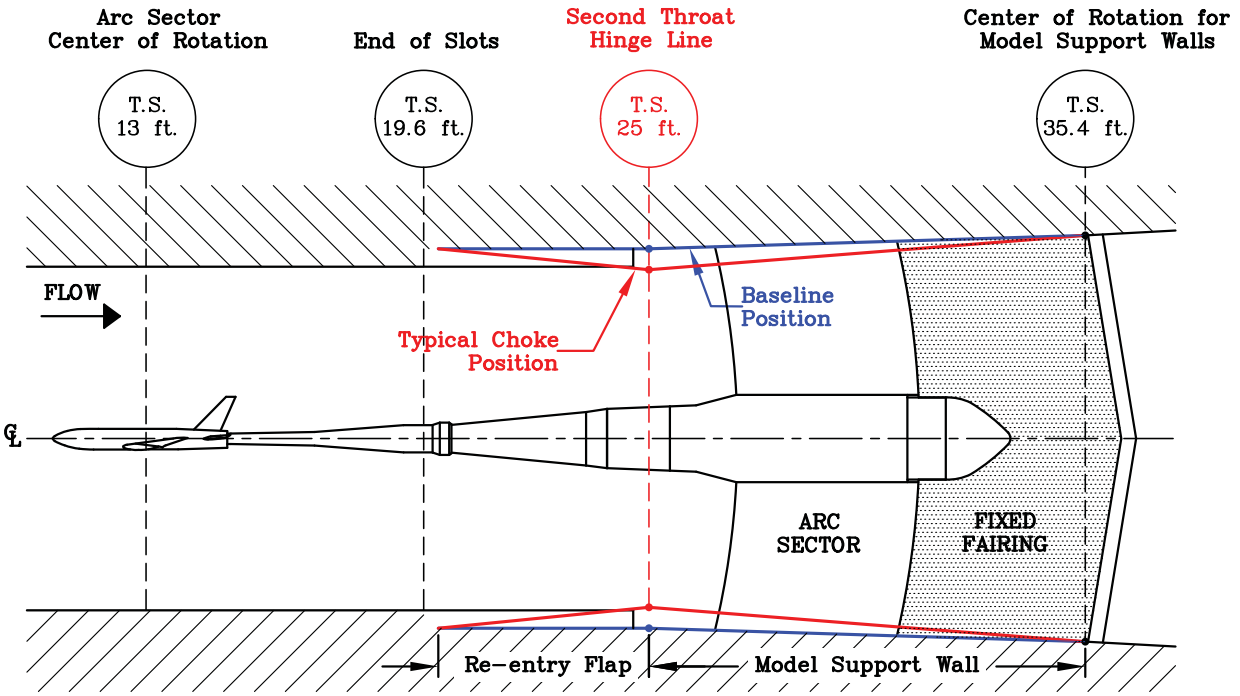

(b) Side View

Figure 5. Top view (a) and side view (b) of the existing second throat capability at the NTF using the re-entry flaps and model support walls.

III. Experimental Setup

A. Test Articles

Two aircraft models were tested in the NTF to evaluate the effectiveness of the second throat in reducing the Mach number variability. The models were different in overall geometric size and total blockage characteristics.

The NASA Common Research Model[21] (CRM) shown in Figure 6 was designed as an open geometry high-speed wing configuration to be used for CFD validation exercises as part of the AIAA CFD Drag Prediction Workshop (DPW). The configuration consists of a contemporary supercritical transonic wing and a fuselage that is representative of a wide-body commercial transport aircraft. The CRM is designed for a cruise Mach number of $M_{\infty} = 0.85$ and a corresponding design lift coefficient of $C_{L} = 0.5$. A 2.7%-scale full-span model of the CRM was built and tested in the NTF in the recent past[22] and the same model was used for the second throat evaluation experiments discussed here.

Figure 6. Photograph of the NASA Common Research Model in the NTF.

The NTF full-scale Pathfinder-I (PF-I) model shown in Figure 7 is representative of a subsonic, energy-efficient transport with a wide-body fuselage and a supercritical wing. It is a full-span model designed for a cruise Mach number of $M_{\infty} = 0.82$ at a cruise lift coefficient of $C_{L} = 0.55$. The Pathfinder-I model has been used extensively in the NTF, not only in the checkout of tunnel systems but also as a research model for high Reynolds number and cryogenic flow phenomena.[23] In recent years, it has been the check standard model at the NTF to assess and track data repeatability at yearly time intervals and especially after tunnel modifications and upgrades.[24,25]

The 2.7%-scale CRM model has a wingspan of 62.47 inches, a max fuselage diameter of 6.59 inches, and a mean aerodynamic chord of 7.45 inches, while the NTF PF-I model is smaller and has a wingspan of 52.97 inches, a max fuselage diameter of 5.75 inches, and a mean aerodynamic chord of 5.74 inches. Table 1 lists other model and wing reference dimensions for both models and Figure 8 provides a visual size comparison between the two models.

Figure 7. Photograph of the Pathfinder-I Model in the NTF.

Due to their size differences, the NASA CRM and the NTF PF-I models also have different blockage interference factors. During the second throat evaluation experiments, it was postulated that the wall settings and effectiveness of the second throat could change due to the different blockage ratios presented by the different size models. This postulation would affect the number of additional tunnel calibration points needed for the choked tunnel configuration as the facility continued on the path to integrating the second throat into its main operations.

The total blockage, ε, is the sum of the solid blockage, ε_{SB}, and the wake blockage, ε_{WB}. The solid and wake blockage components can be estimated using Equation 2 and Equation 3, respectively, using the maximum frontal cross-sectional area of the test article, the wing reference area of the test article, the NTF test section cross-sectional area, and the profile or minimum drag coefficient of the test article.[26] The blockage factors for the NASA CRM and NTF PF-I models at a Mach number of $M_{\infty} = 0.85$ are summarized in Table 2.

$$\varepsilon_{SB} = \frac{A_{max}}{\left(1 - M_{\infty}^{2}\right) A_{TS}} \tag{2}$$

$$\varepsilon_{WB} = \frac{S_{ref}\, C_{D_0}}{4\left(1 - M_{\infty}^{2}\right) A_{TS}} \tag{3}$$

Table 1. Model and wing reference dimensions for NASA Common Research Model and NTF Pathfinder-I model.

Parameter	NASA CRM	NTF PF-I
Scale	0.027	1
Design Mach Number (M_∞)	0.85	0.82
Design Lift Coefficient (C_L)	0.5	0.55
Wingspan (b)	62.47 in	52.97 in
Wing Reference Area (S_{ref})	3.01 ft^2	1.988 ft^2
Mean Aerodynamic Chord ($\bar{c}$)	7.45 in	5.74 in
Aspect Ratio ($\mathcal{AR}$)	9.0	9.8
Leading Edge Sweep	35°	35°
Taper Ratio	0.275	0.313
Wing Maximum Thickness Ratio	0.154	0.145
Fuselage Max Diameter	6.59 in	5.75 in
Fuselage Length	66.73 in	50 in
Model Volume	1.23 ft^3	0.92 ft^3
Max Frontal Cross-sectional Area	0.41 ft^2	≈0.32 ft^2

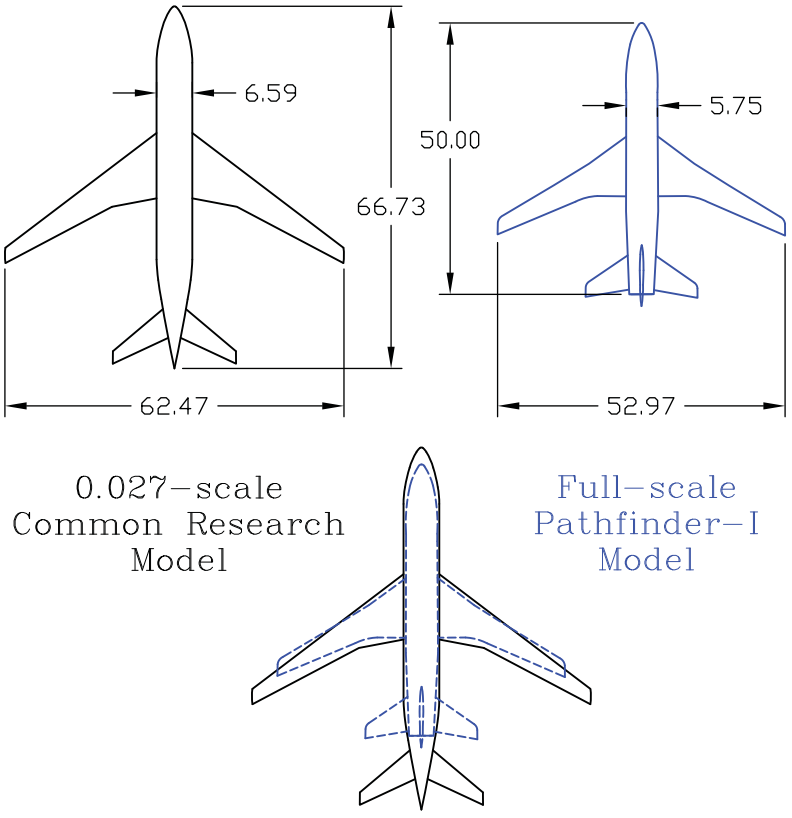

Figure 8. Geometric comparison between NASA CRM and NTF PF-I models. Linear dimensions in inches.

Table 2. Blockage interference factor estimates at $M_\infty = 0.85$ for NASA CRM and NTF PF-I models.

Parameter	NASA CRM	NTF PF-I
Solid Blockage Factor (ε_{SB})	0.022	0.017
Wake Blockage Factor (ε_{WB})	0.00058	0.00067
Total Blockage Factor (ε)	0.0226	0.0177

B. Instrumentation and Data System

The Mach Measurement System (MMS) at NTF is based on simultaneous measurements of the total and static pressure in the tunnel as shown in Figure 9. The total pressure is measured from a pitot tube in the contraction and an alternate measurement can be obtained from a pitot tube located in the bottom of the settling chamber. The reference static pressure is measured in the plenum and is corrected to freestream static pressure by the tunnel calibration. The transducers for this system are optimized for the approximately nine atmosphere pressure range of the facility. Two Fluke® 7052i absolute gauges (150 psia and 50 psia ranges) are used for total pressure measurements and two Fluke® 7052i differential gauges (55 psid and 14 psid ranges) are used for the static pressure measurements.[1] These gauges are automatically selected based on the optimal pressure range needed for the measurement. The digital output of these gauges are low pass filtered at 1 hertz. The total and static pressure measurements are used with the total temperature measurement to calculate the reference Mach number. The reference Mach number is then corrected to the freestream Mach number in the test section using the tunnel calibration.

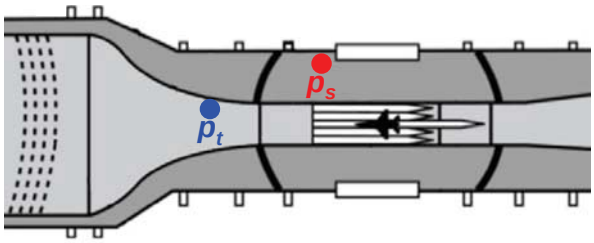

Figure 9. Total and static pressure measurement locations in the NTF.

The NTF-118A balance was used to acquire force and moment data on both the CRM and PF-1 models. The NTF-118A is a 6-component strain-gauge balance fabricated from Aermet 100 and can be used at both warm and cryogenic temperatures. Table 3 lists the load ranges and accuracies of the NTF-118A balance.

There were two independent data acquisition systems utilized for this series of test, the NTF Data Acquisition System (DAS) and the NTF Dynamic Data Acquisition System (DDAS). The majority of this paper will be focused on data collected by the DAS system. The NTF DAS and DDAS[27,28] are based on the Jacobs Technology® Test SLATE (Software for Laboratory and Automated Test Environments) software,[29] which is also in use at other LaRC facilities. For both experiments, the DAS data were acquired at 400 Hz over 12 seconds. The DAS data included tunnel parameters data, model force and moment data, model orientation data, and model surface pressure data. The DDAS data, which included model force and moment data and tunnel unsteady pressure data, were acquired at 12,800 Hz over a 12 second period. Unfortunately, DDAS data were not available for the Pathfinder-I experiment due to a software problem. Table 4 summarizes the data acquisition parameters for the two data systems.

Table 3. NTF-118A balance calibration load ranges and accuracies.

Component	Calibration Range	Accuracy
Normal Force	6,520 lbf	±3.91 lbf
Axial Force	700 lbf	±0.7 lbf
Pitching Moment	12,800 in-lbf	±11.5 in-lbf
Rolling Moment	8,150 in-lbf	±10.6 in-lbf
Yawing Moment	6,400 in-lbf	±9.6 in-lbf
Side Force	4,000 lbf	±6.0 lbf

Table 4. NTF standard (DAS) and dynamic (DDAS) data system acquisition parameters.

DAS	Sampling Frequency	Sampling Period
Standard	400 Hz	12 sec
Dynamic	12,800 Hz	12 sec

IV. Results

Results from two recent experiments in the NTF with the NASA Common Research Model and the NTF Pathfinder-I model are presented in this section. While there were many investigations happening concurrently during these tests, the results here focus only on the baseline tunnel configuration and the choked tunnel configuration with no vortex generators installed in the entry to the high-speed diffuser. For the choked tunnel configuration, the second throat was set for a test section choke Mach number of $M_\infty = 0.9$. Table 5 lists the model support wall and re-entry flap settings for the baseline tunnel configuration and the choked tunnel configuration. The angles are defined as positive for rotating away from the test section and negative for rotating into the test section.

Table 5. Model support wall and re-entry flap settings for the baseline and choked tunnel configurations.

Tunnel Configuration	**Model Support Walls**	**Re-entry Flaps**
Baseline	-1.76°	0°
Choked for $M_\infty = 0.9$	-3.53°	3.67°

The PF-I experiment was conducted only in air mode at 120 °F, while the CRM experiment was mostly conducted in air mode at 120 °F, but also acquired data at cryogenic conditions at temperatures of -50 °F and -250 °F. The CRM experiment focused mostly at Mach numbers of $M_\infty = 0.7$ and $M_\infty = 0.85$ with limited data at $M_\infty = 0.87$. The PF-1 experiment acquired data at Mach numbers between $M_\infty = 0.7$ and $M_\infty = 0.88$ in increments of 0.05 between $M_\infty = 0.7$ and $M_\infty = 0.8$ and increments of 0.01 between $M_\infty = 0.84$ and $M_\infty = 0.88$. Although there were similar Mach numbers between the two experiments, the dynamic pressure conditions and Reynolds number were different. Table 6 lists the tunnel conditions for the two experiments.

Table 6. Tunnel conditions for the CRM and PF-I experiments.

Model	M_∞	T_t, **°F**	p_t, **psia**	q_∞, **psf**	$Re, 10^6$
PF-I	0.7	120	21.5	766	2.45
	0.75	120	21.5	840	2.55
	0.80	120	21.5	910	2.64
	0.82	120	21.5	938	2.67
	0.84	120	21.5	964	2.70
	0.85	120	21.5	977	2.72
	0.86	120	21.5	990	2.73
	0.87	120	21.5	1002	2.74
	0.88	120	21.5	1014	2.76
CRM	0.7	120	33.8	1204	5.0
	0.85	120	30.5	1386	5.0
	0.87	120	30.2	1408	5.0
	0.85	-50	38.1	1732	10.0
	0.7	-250	32.3	1150	19.8
	0.85	-250	28.9	1311	19.8
	0.87	-250	28.6	1330	19.8

A. Sonic Conditions at Throat

NTF possesses a number of static pressure rows on the test section floor and ceiling as well as the sidewalls as shown in Figure 10. However, at the present time, only Row 9 on the far sidewall has pressure taps that extend beyond the test section and into the existing second throat area. Figure 11 shows an example of the local Mach numbers on the far sidewall in Row 9 for the baseline tunnel configuration and the choked tunnel configuration at $M_\infty = 0.85$ and $M_\infty = 0.88$ with the PF-I model at 0° angle of attack. The local Mach numbers change a little as a function of angle of attack, but not significantly and are therefore not presented. It is clear that the second throat achieves a sonic condition in the choked tunnel configuration as expected. The local Mach number achieves a maximum near the pressure orifice at station 25.44 feet, therefore the data at this station are used to determine when the second throat has achieved a sonic condition.

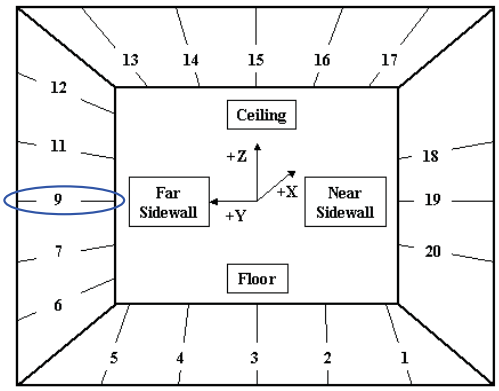

Figure 10. Layout of NTF wall static pressure orifice rows. Currently, Row 9 is the only row that reaches past the second throat at station 25 feet.

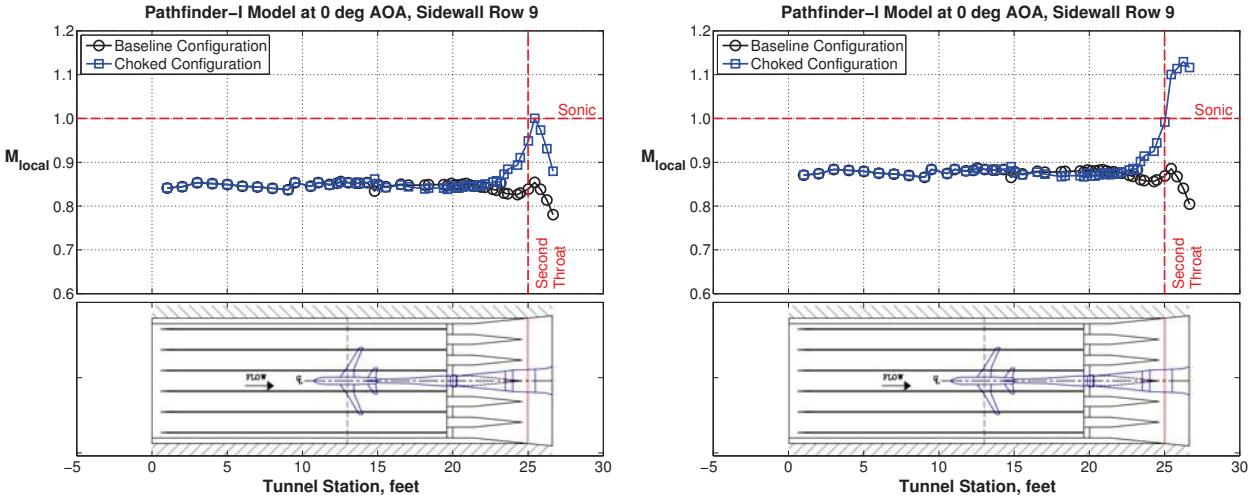

(a) $M_\infty = 0.85$ (b) $M_\infty = 0.88$

Figure 11. Comparison of the local Mach number on Row 9 on the far sidewall between the baseline tunnel configuration and the choked tunnel configuration for the Pathfinder-I Model at (a) $M_\infty = 0.85$ and (b) $M_\infty = 0.88$.

Figure 12 shows the local Mach number on the far sidewall at station 25.44 feet as a function of freestream Mach number in the baseline tunnel configuration and the choked tunnel configuration for the PF-I model. In the choked tunnel configuration set for a choke Mach number of $M_\infty = 0.9$ in the test section, the second throat achieves a sonic condition for freestream Mach numbers $M_\infty \geq 0.85$. It is also clear that as the freestream Mach number approaches the choke Mach number, the strength of the shock at the second throat increases.

If the choked tunnel configuration is changed to set different choke Mach numbers, the local Mach data at station 25.44 feet of Row 9 is the only data source, currently, that can be used to ensure a sonic condition at the throat. However, there are plans to add pressure taps to the other centerline rows on the near sidewall (Row 19), the floor (Row 3), and the ceiling (Row 15) to extend past the end of the test section and into the existing second throat area. The additional pressure taps would provide data to determine the uniformity and symmetry of the shock at the second throat. This information would be valuable for understanding the behavior of the second throat with different lifting models in the tunnel.

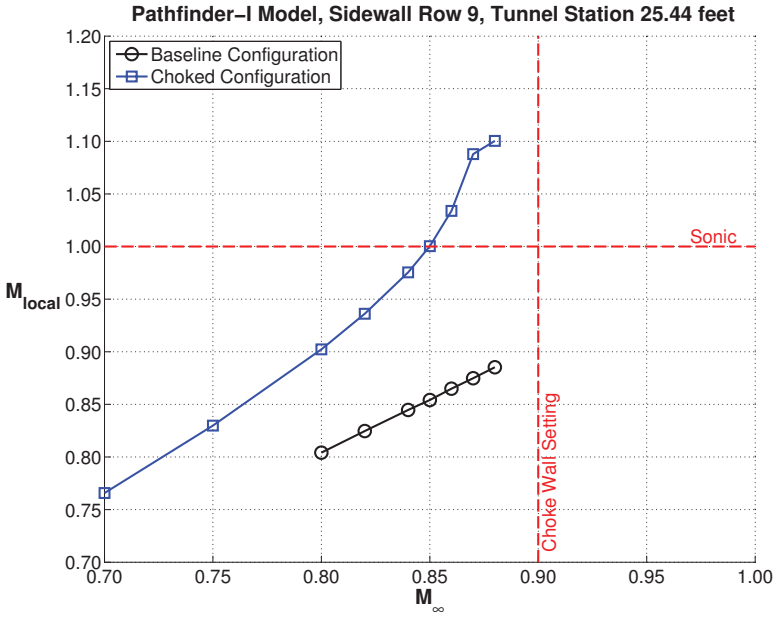

Figure 12. Comparison of the local Mach number on the far sidewall at station 25.44 feet as a function of freestream Mach number in the baseline tunnel configuration and the choked tunnel configuration for the Pathfinder-I Model.

B. Mach Variability

In both experiments, the NTF DAS acquired data at 400 Hz over 12 seconds for each data point in a pitch-pause polar. All samples within a data point are used to examine the variability in the freestream Mach number. The goal, as stated earlier, is to reduce the Mach variation within a data point to $M_\infty \pm 0.0005$, which corresponds to a range (maximum − minimum) of $R(M_\infty) = 0.001$. Figure 13 shows examples of the Mach variation at $M_\infty = 0.85$ for the CRM model for both the baseline tunnel configuration and the choked tunnel configuration. All of the samples within a data point are plotted as a solid line while the average of all of the samples within a data point are plotted as filled circles. Note that the trace is not contiguous, i.e., there is a time delay between each data point as the model is traversed to the next angle of attack and the tunnel control system adjusts the Mach number accordingly. The range $R(M_\infty)$ is also calculated for every angle of attack data point with the desired variation goals plotted for reference.

For the baseline tunnel configuration, the mean Mach number value across the entire pitch polar does not meet the desired goals, although it is within the facility quoted accuracy of $M_\infty \pm 0.001$. Furthermore, the variation within each data point is sometimes quite large. Note that in all of these runs, the control system is allowed to adjust the inlet guide vanes for small adjustments to the Mach number. The controller will respond to pressure fluctuations in the test section and can sometimes exacerbate the situation by responding to pressure fluctuations that it cannot keep up with.

For the choked configuration, the Mach number variation within a data point is noticeably reduced as expected, and almost all of the mean values fall within the desired goal limits. The remaining variation that lie outside of the limits can be reduced further by setting the choke condition closer to the Mach number of interest. As the shock at the second throat gets stronger, its effectiveness increases at blocking upstream-moving disturbances. This can be seen in Figure 14 in the comparison between the Mach number variation at $M_\infty = 0.85$ and $M_\infty = 0.88$ for the choked tunnel configuration with the PF-I model. The second throat is set to fully choke at a test section Mach number of $M_\infty = 0.9$ and it is clear that the Mach number variation at $M_\infty = 0.88$ is drastically reduced from even the $M_\infty = 0.85$ variation levels. However, there are consequences for running close to the choke Mach number because of the location of the existing second throat at the end of the test section, which will be mentioned briefly in a later section. Therefore, it is better to run at Mach numbers below the choke setting and use other techniques, namely control system improvements and conditional sampling methods, to reduce any remaining variation outside of the goal limits.

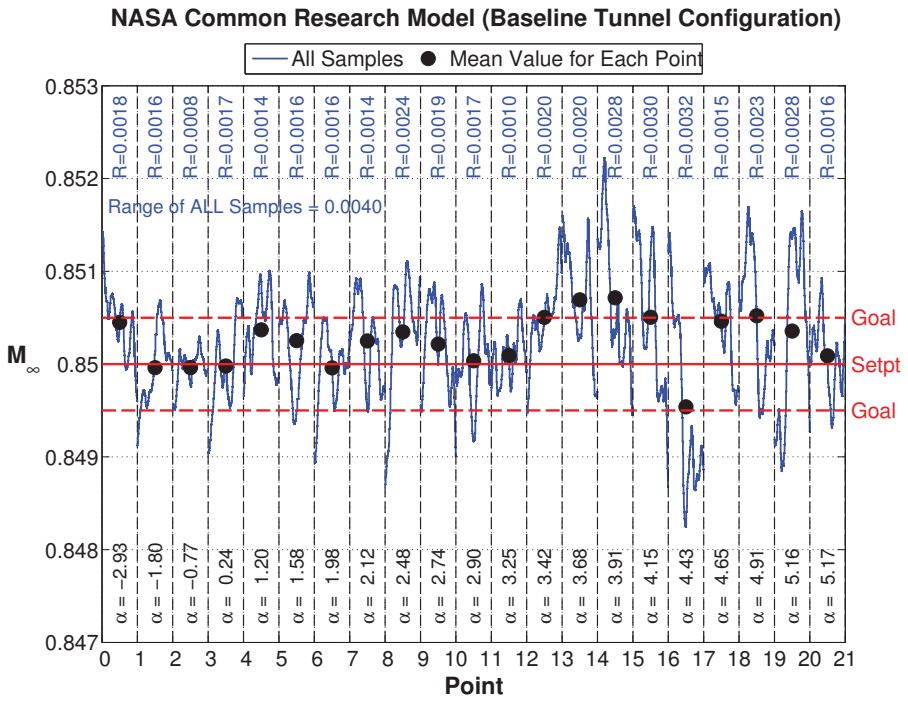

(a) Baseline tunnel configuration

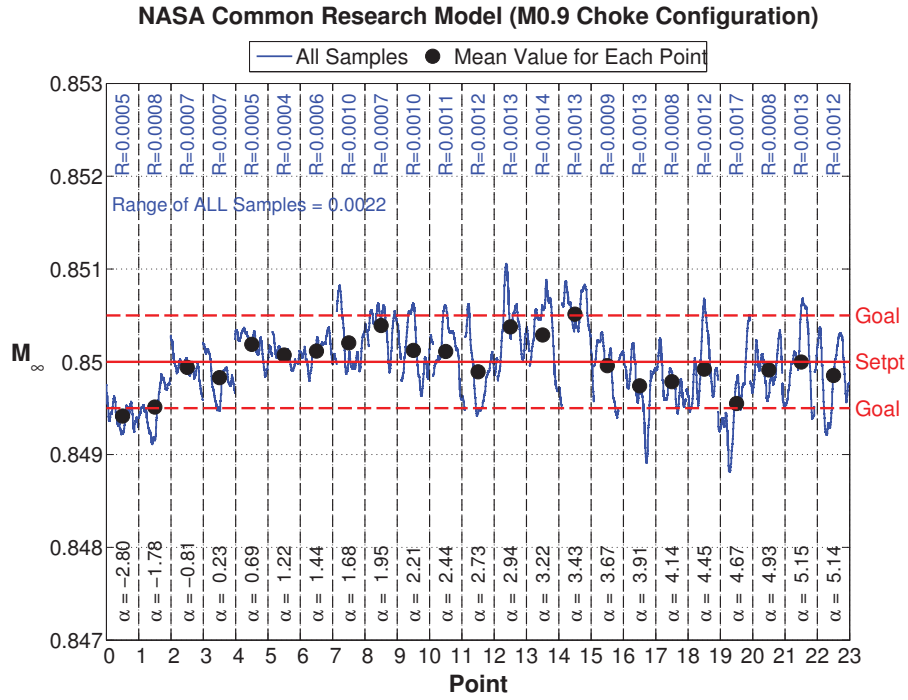

(b) Choked tunnel configuration

Figure 13. Comparison of the Mach number variation at $M_\infty = 0.85$ between the (a) baseline tunnel configuration and the (b) choked tunnel configuration for the Common Research Model.

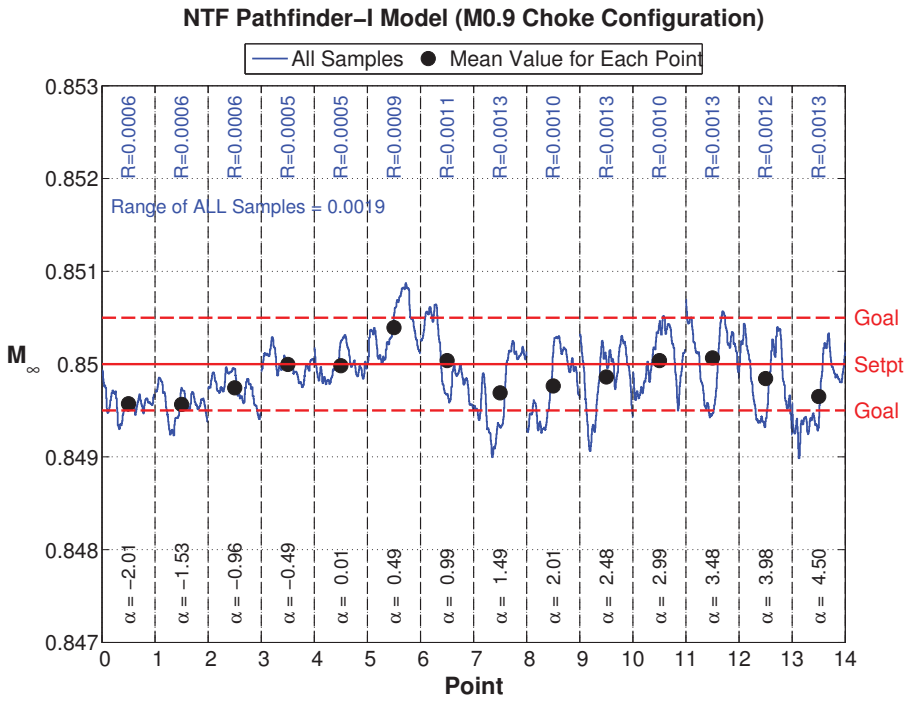

(a) $M_\infty = 0.85$

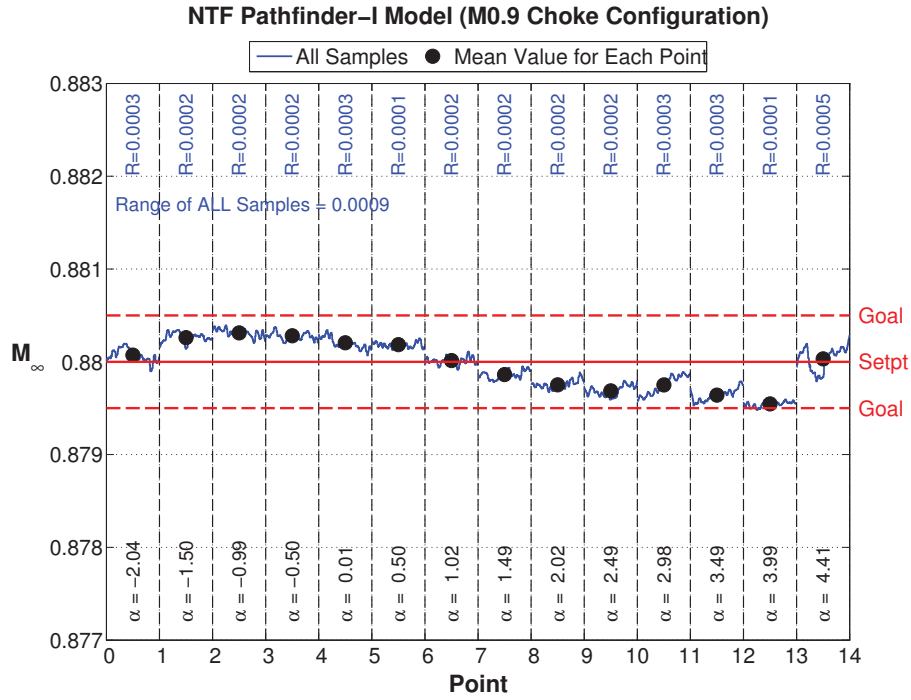

(b) $M_\infty = 0.88$

Figure 14. Comparison of the Mach number variation at (a) $M_\infty = 0.85$ and (b) $M_\infty = 0.88$ in the choked tunnel configuration for the Pathfinder-I Model.

From inspection of the plots in Figures 13 and 14, it can be seen that the Mach number variation within a data point increases with angle of attack. This is summarized in Figure 15 for the baseline tunnel configuration and choked tunnel configuration with both the CRM model and the PF-I model. In the baseline tunnel configuration for both models, there is a clear upward trend of the Mach variation with angle of attack. In the choked tunnel configuration, the overall Mach variation levels have been reduced with many values within the goal limits. Furthermore, the trend in Mach variation with angle of attack is also reduced and almost eliminated, suggesting that the model wake is nearly decoupled from the high-speed diffuser by the barrier set up by the second throat.

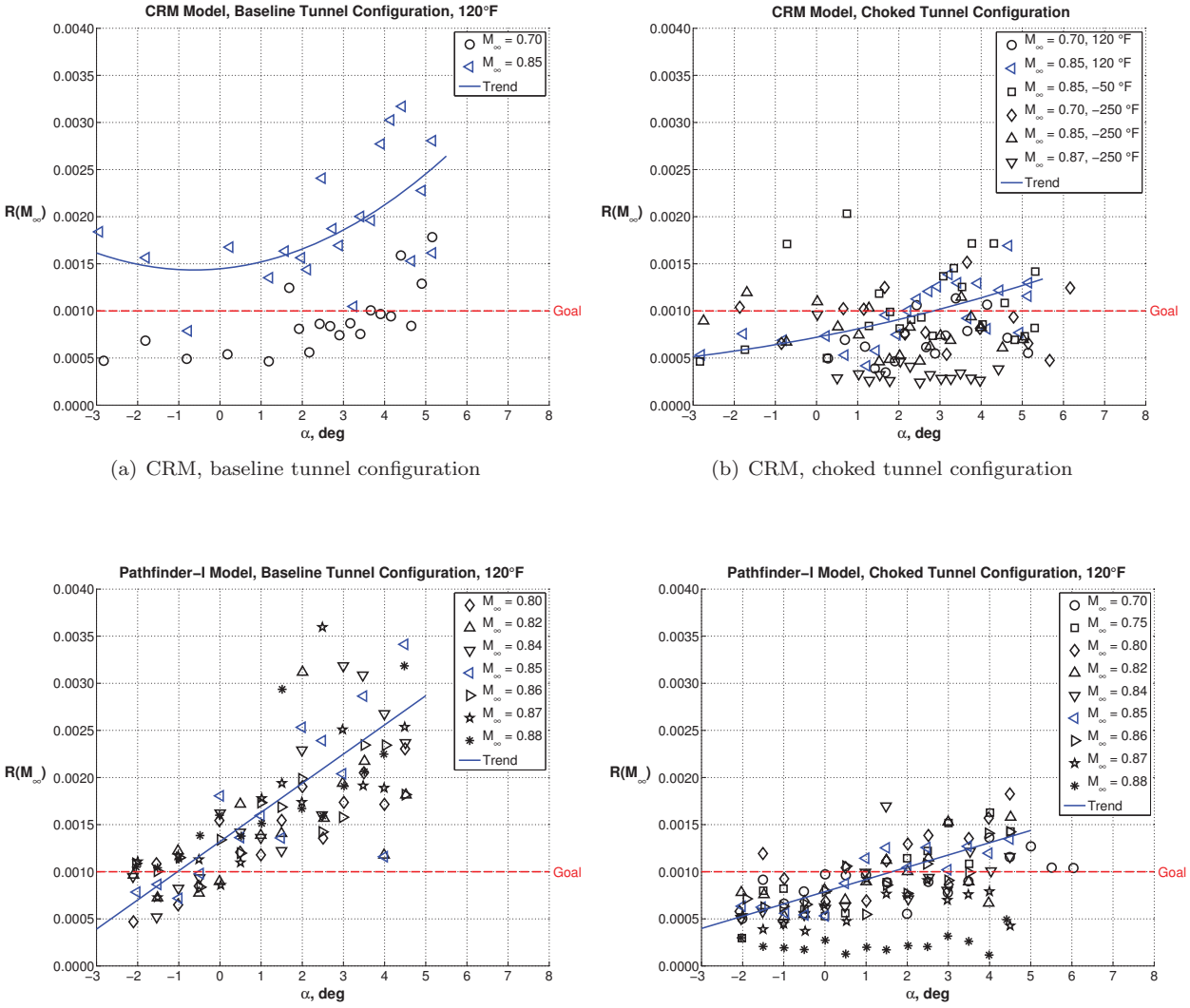

(a) CRM, baseline tunnel configuration

(b) CRM, choked tunnel configuration

(c) PF-I, baseline tunnel configuration

(d) PF-I, choked tunnel configuration

Figure 15. Comparison of the Mach number variation as a function of angle of attack in the baseline tunnel configuration and the choked tunnel configuration for both the Common Research Model and the Pathfinder-I Model.

Finally, because the correlation of the Mach variation with angle of attack has been mostly eliminated in the choked tunnel configuration, the remaining correlation is with Mach number. Figure 16 summarizes the Mach variation trend as a function of freestream Mach number for the baseline tunnel configuration and the choked tunnel configuration with both the CRM model and the PF-I model. The $R(M_\infty)$ quantity is averaged across all angles of attack in each polar and plotted against freestream Mach number. This plot includes data mostly in air mode at 120 °F for the two models, but also includes some cryogenic data at -50 °F and -250 °F for the CRM model. It also includes empty tunnel data in air mode with only the nose bullet

installed with the tunnel in the choked configuration. The choked empty tunnel data provides a minimum level of Mach variation that can be achieved in the tunnel. Trendlines are also provided for clarity and it is clear that in the baseline tunnel configuration, the Mach variation increases with increasing Mach number and in the choked tunnel configuration, the Mach variation decreases asymptotically as the freestream Mach number approaches the choke Mach number. From this plot, it can be seen that the Mach variation levels at $M_\infty = 0.85$ in the choked tunnel configuration demonstrated about a 40-45% reduction from the baseline tunnel configuration levels and are within the desired goals.

It is also important to note that Mach variation levels do not seem to depend on the model installed in the tunnel. Even though the CRM and PF-I models have different blockage interference factors, the Mach variation levels were very similar between the two models in both the baseline and choked tunnel configurations. However, the two models are still lift-generating models. This observation would need to be verified for a model with a larger blockage factor, such as a large half-span model, or for a model with a smaller blockage factor, such as a fighter configuration, or for a non-lift-generating model, such as a launch vehicle.

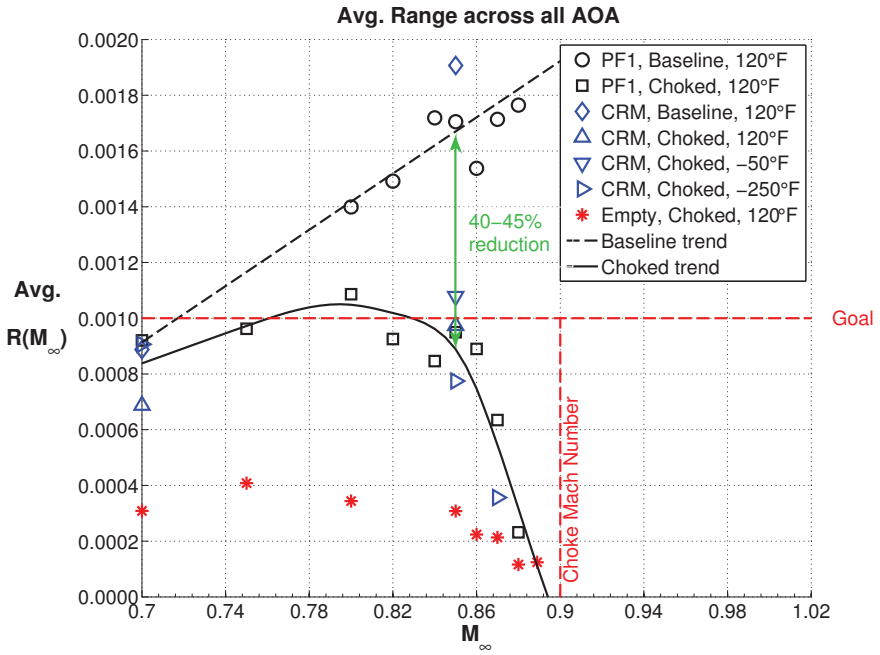

Figure 16. Comparison of the Mach number variation as a function of Mach number in the baseline tunnel configuration and the choked tunnel configuration for both the Common Research Model and the Pathfinder-I Model.

C. Correlation Between Mach Number and Drag

The improvements to the Mach number stability in the NTF through the use of the existing second throat can help to improve the drag repeatability if it can be demonstrated that a relationship exists between Mach number variability and drag variability. For the CRM model tested in the NTF, such a relationship exists. The model wake is the primary driver of low frequency flow disturbances in the tunnel and the disturbances increase with angle of attack. These low frequency disturbances excite modes in the high-speed diffuser and adversely affect Mach number stability. The Mach control system in the tunnel is unable to overcome these disturbances. It was shown in Figure 15 that the choked tunnel configuration nearly decouples the model wake from the high-speed diffuser since the trend in Mach variation with angle of attack was significantly reduced. This effect can also be seen in the balance axial force data acquired by the DDAS for the CRM model. Figure 17 shows the low frequency content of the balance axial force fluctuations as a function of angle of attack at $M_\infty = 0.85$ in the baseline tunnel configuration and the choked tunnel configuration for the CRM model. The axial force fluctuation spectra were integrated between 0.125 Hz and 3 Hz to isolate

the low frequency, long period content. It is clear that the trend in low frequency axial force fluctuations with angle of attack was reduced in the choked tunnel configuration similar to the Mach variation.

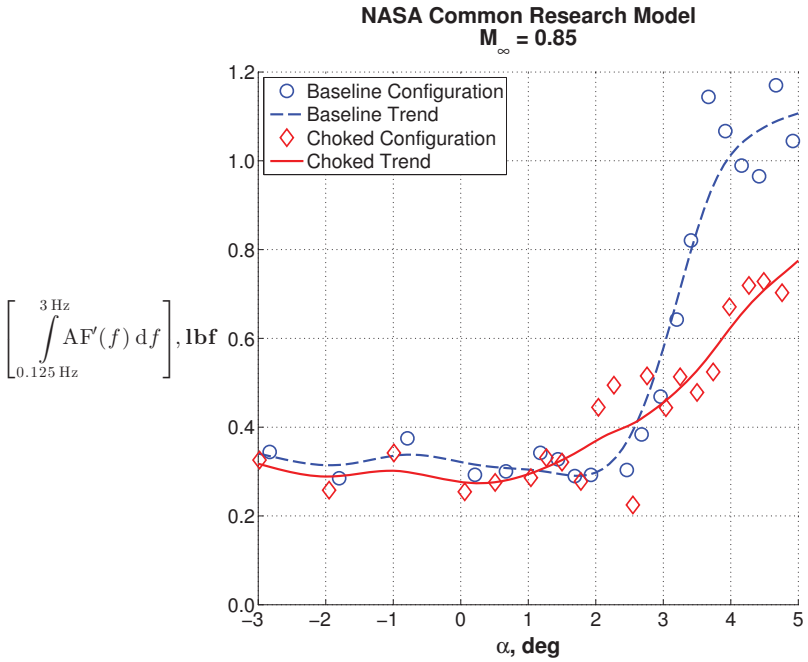

Figure 17. Comparison of the low frequency content of the balance axial force fluctuations as a function of angle of attack at $M_\infty = 0.85$ in the baseline tunnel configuration and the choked tunnel configuration for the Common Research Model.

A direct correlation between Mach number variation and axial force variation was determined for the CRM model by examining the individual data samples acquired from the DAS. The axial force data and Mach number data were time-aligned to take into account delays in the total and static pressure measurements, which resulted in the revelation of a strong correlation between Mach number variation and axial force variation at higher angles of attack. This can be seen in Figure 18, which shows the balance axial force and Mach number measurements as a function of time for the CRM model at $M_\infty = 0.85$ and an angle of attack of 4.9°. It is clear that the two measurements are highly correlated in both the baseline tunnel configuration and the choked tunnel configuration.

The correlation between Mach number and axial force were examined at all angles of attack by calculating the Pearson correlation coefficient. This coefficient is a measure of the linear correlation between two variables that are believed to be independent of one another. The coefficient value can range from +1 to −1, with 0 indicating no correlation and values of +1 or −1 indicating complete dependance. Linear dependence between two variables suggests one of the variables has high influence on the other. Figure 19 shows the Pearson correlation coefficient between Mach number and axial force as a function of angle of attack at $M_\infty = 0.85$ for the CRM model in both the baseline tunnel configuration and the choked tunnel configuration. For low angles of attack up to about 2.5°, a strong correlation between Mach number and axial force does not exist. However, for angles of attack at or above 3°, there is significant correlation between Mach number and axial force. This may be due in part to the fact that the CRM wing was designed for $M_\infty = 0.85$ at a lift coefficient $C_L = 0.5$, which corresponds to roughly 3° angle of attack. At $M_\infty = 0.85$, the lift coefficient and pitching moment coefficient experience a break or slope change at around 3° angle of attack.[22] Furthermore, at $C_L = 0.5$, the beginning of the drag rise occurs at about $M_\infty = 0.85$.[21] In the drag rise region, it is obviously very important to control Mach number to tight tolerances because small variations in Mach number can lead to large variations in drag.

The drag repeatability results from these experiments are out of the scope of this paper and will not be shown here, but through the use of the existing second throat, conditional sampling techniques, and control system improvements, the drag repeatability levels were reduced to within the 0.5 drag count goal limits for the entire angle of attack range.

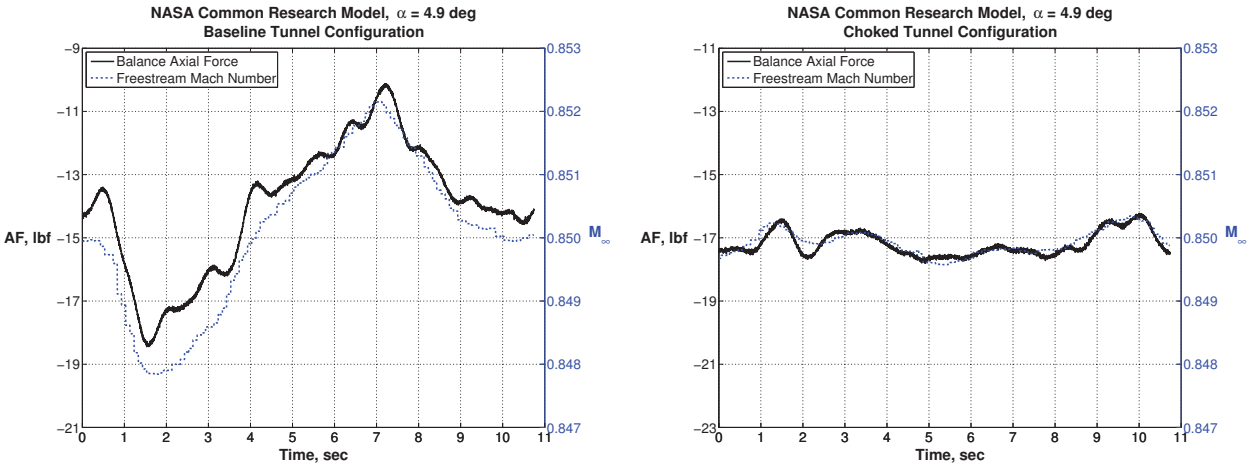

(a) Baseline tunnel configuration

(b) Choked tunnel configuration

Figure 18. Comparison of the time-aligned Mach number and balance axial force measurements at $M_\infty = 0.85$ and $\alpha = 4.9°$ for the Common Research Model in the (a) baseline tunnel configuration and the (b) choked tunnel configuration.

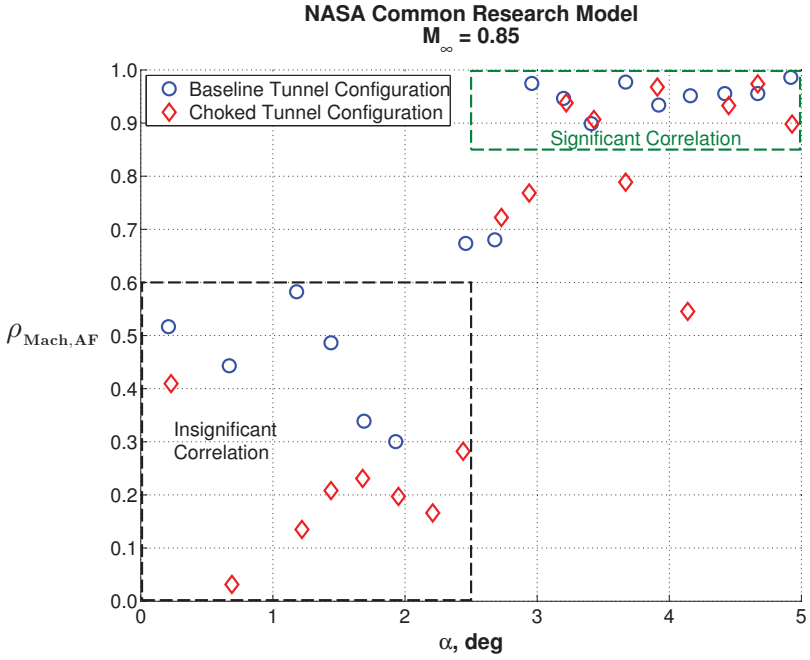

Figure 19. Comparison of the Pearson correlation coefficient between Mach number and axial force as a function of angle of attack at $M_\infty = 0.85$ in the baseline tunnel configuration and the choked tunnel configuration for the Common Research Model.

D. Consequences of Using Existing Second Throat

There are a few known consequences to using the existing second throat at the end of the test section, which will be discussed briefly here. As mentioned earlier, second throats are usually employed downstream of the test section and usually behind the model support structure or arc sector. The location of the existing second throat at NTF (at the end of the test section but upstream of the arc sector) places a shock of varying strength on the stub sting and can cause undesired model dynamics. One of the main frequency modes of the

arc sector and model support system in the y-direction (side-to-side dynamics) at the NTF occurs around 10-12 Hz.[30] Figure 20 shows a comparison of the fluctuating balance side force and normal force components between the baseline tunnel configuration and the choked tunnel configuration at 4.5° angle of attack for the CRM model at $M_\infty = 0.85$ and $M_\infty = 0.87$. The spectral data are plotted on similar scales for easier comparison between balance components, tunnel configurations, and Mach numbers. In the choked tunnel configuration, the dominant arc sector mode at 10-12 Hz is excited by the shock at the second throat, as shown in the balance side force component, for both $M_\infty = 0.85$ and $M_\infty = 0.87$. As the freestream Mach number approaches the choke Mach number, the shock strength at the second throat increases and continues to excite this mode further, causing increased model dynamics and possibly negating any benefit to the drag repeatability gained from the increase in Mach stability.

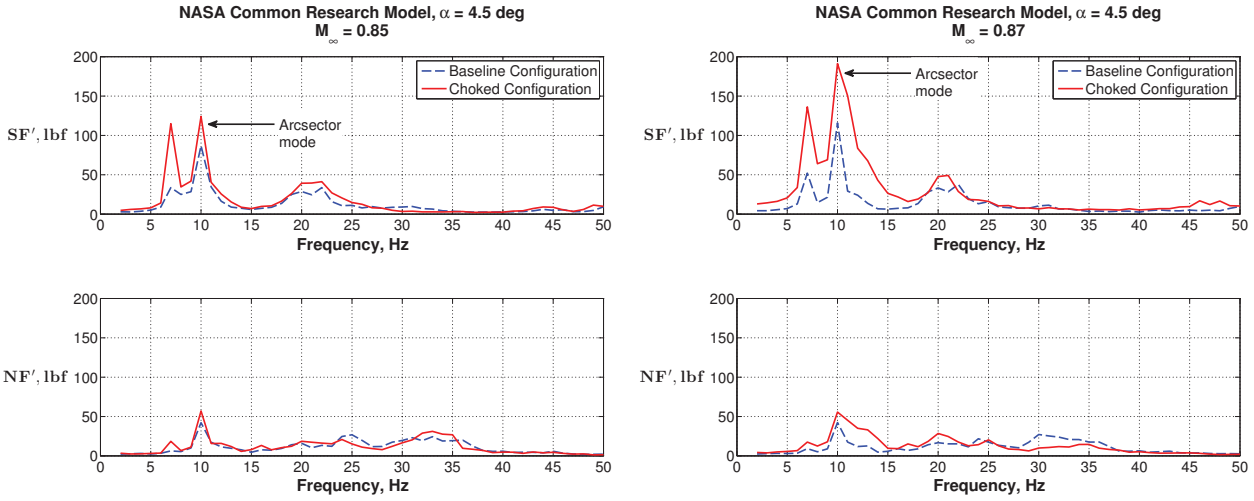

(a) $M_\infty = 0.85$ (b) $M_\infty = 0.87$

Figure 20. Comparison of the fluctuating balance side force and normal force components between the baseline tunnel configuration and the choked tunnel configuration at 4.5° angle of attack for the Common Research Model at (a) $M_\infty = 0.85$ and (b) $M_\infty = 0.87$.

Additionally, the location of the existing second throat at the end of the test section will have effects on the tunnel calibration. As the second throat is engaged, it may change the calibrated test section Mach number and Mach number distribution. Consequently, an update to the tunnel calibration will be needed for transonic Mach numbers across all tunnel conditions for the choked tunnel configuration, or at the very least, an investigation into the magnitudes of the effects. During the recent tunnel calibration check-out test, data were acquired with the centerline pipe calibration probe over a wide range of tunnel conditions (Mach number, total pressure, and total temperature). As part of this test, the choked tunnel configuration was employed at a limited number of tunnel conditions to determine the effect it might have on the test section Mach number and Mach number distribution. Preliminary results show that there is a small effect to both the calibrated test section Mach number and the Mach number distribution.

The facility is currently working towards putting the second throat into standard operations at the tunnel and there are plans to perform the update to the tunnel calibration for the choked tunnel configuration. Further investigations and check-out experiments will be needed to fully comprehend all aspects of employing the second throat before it will be put into production mode at the facility. There are also preliminary designs for a second throat mechanism downstream of the arc sector to avoid the problems mentioned here, but the project is still in the initial stages of securing funding.

V. Concluding Remarks

The focus of this paper has been on the Mach number stability improvements at the NTF provided by the existing second throat capability at the end of the test section. Data from two recent experiments at the NTF with the NASA Common Research Model and the NTF Pathfinder-I model were analyzed to verify that a sonic condition was achieved at the second throat and to quantify the Mach number variation in the test section in the baseline tunnel configuration and the choked tunnel configuration. Results show that the choked tunnel configuration reduces the Mach variation by about 40-45% at $M_\infty = 0.85$ and the Mach variation reduces significantly as the freestream Mach number approaches the choke Mach number.

Results also showed that the existing second throat was effective in reducing the trend with angle of attack for the Mach number variations and low frequency balance axial force fluctuations, suggesting that the model wake was nearly decoupled from the high-speed diffuser. Significant correlation between Mach number variations and axial force variations were discovered for higher angles of attack at $M_\infty = 0.85$ for the CRM model, most likely due to the beginning of drag rise at that condition.

However, there are some consequences to using the existing second throat capability at the end of the test section. The shock produced by the second throat is very near the model support stub sting and can excite known dynamic modes of the arc sector causing increased model dynamics. The model dynamics will increase as the freestream Mach number approaches the choke Mach number and can possibly negate any performance benefit in drag repeatability gained from the increased Mach stability in the test section. Furthermore, the choked tunnel configuration can affect the calibrated test section Mach number and Mach number distribution. An update to the tunnel calibration for the choked tunnel configuration would be needed before the capability is put into production mode at the facility.

As part of the NTF Facility Improvements and Data Optimization (FIDO) project, the facility is working to enable the use of the existing second throat for all tunnel conditions and different types of full-span and semi-span models. While a preliminary design exists for installing a second throat downstream of the arc sector in a more optimum location, it would most likely be cost-prohibitive. Regardless, further experiments and investigations are needed to fully comprehend the benefits and drawbacks of using the existing second throat capability, but the initial results look very promising. The strategy, as exemplified in this paper, is to use the existing second throat to reduce Mach variability levels and then use conditional sampling techniques and control system improvements to ultimately reduce the drag repeatability levels to within 0.5 drag counts.

Acknowledgements

The data acquired during the experiments using the CRM and PF-I models were acquired as part of the NTF STARBUKS and FIDO projects under the NASA Aeronautics Test Program.

Disclaimer of Endorsement

References

[1]Paryz, R. W., "Subsonic Transonic Applied Refinements By Using Key Strategies - STARBUKS In the NASA Langley Research Center National Transonic Facility," AIAA Paper 2014-1481, AIAA, January 2014.

[2]Jones, G. S., Balakrishna, S., Demoss, J. A., Goodliff, S. L., and Bailey, M. M., "Influences of Models on the Unsteady Pressure Characteristics of NTF (Invited)," AIAA Paper 2015-, AIAA, January 2015.

[3]Acosta, D. M., Guynn, M. D., Wahls, R. A., and Rosario, R. D., "Next Generation Civil Transport Aircraft Design Considerations for Improving Vehicle and System-Level Efficiency," AIAA Paper 2013-4286, AIAA, 2013.

[4]Wahls, R. A., Adcock, J. B., Witkowski, D. P., and Wright, F. L., "A Longitudinal Aerodynamic Data Repeatability Study for a Commercial Transport Model Test in the National Transonic Facility," NASA TP 3522, NASA Langley Research

Center, August 1995.

[5]Om, D., Curtin, M. M., Bogue, D. R., Witkowski, D. P., and Ball, D. N., "Reynolds Number Effects on a Subsonic Transport at Transonic Conditions (Invited)," AIAA Paper 2001-0909, January 2001.

[6]Curtin, M. M., Bogue, D. R., and Om, D., "Investigation of Transonic Reynolds Number Scaling on a Twin-Engine Transport (Invited)," AIAA Paper 2002-0420, AIAA, January 2002.

[7]Bobbitt-Jr., C. and Everhart, J. L., "Status of the National Transonic Facility Characterization," AIAA Paper 2001-0755, AIAA, January 2001.

[8]King, R. A., Andino, M. Y., Melton, L. P., Eppink, J., Kegerise, M. A., and Tsoi, A., "Flow Disturbance Characterization Measurements in the National Transonic Facility (Invited)," AIAA Paper 2012-0104, AIAA, January 2012.

[9]Dor, J.-B., "The T2 Cryogenic Induction Tunnel in Toulouse," *Special Course on Cryogenic Technology for Wind Tunnel Testing*, No. R-722, AGARD, April 1985, pp. 9–1 to 9–22.

[10]Michel, R., Mignosi, A., and Quemard, C., "The Induction Driven Tunnel at ONERA-CERT : Flow Qualities, Testing Techniques, and Examples of Results," AIAA Paper 1978-767, AIAA, April 1978.

[11]http://www.starcs.se/t1500.aspx, "T1500 - STARCS Transonic Wind Tunnel," .

[12]Torngren, L., Grunnet, J. L., Nelson, D. M., and Kamis, D. N., "The New FFA T1500 Transonic Wind Tunnel - Initial Operations, Calibration, and Test Results," AIAA Paper 1990-1420, AIAA, June 1990.

[13]https://www.etw.de/cms, "European Transonic Windtunnel," .

[14]Green, J. and Quest, J., "A Short History of the European Transonic Wind Tunnel ETW," *Progress in Aerospace Sciences*, Vol. 47, 2011, pp. 319–368.

[15]Cuyler W. Brooks, J., Harris, C. D., and Reagon, P. G., "The NASA Langley 8-Foot Transonic Pressure Tunnel Calibration," NASA TP 3437, NASA Langley Research Center, August 1994.

[16]Harris, C. D., Harvey, W. D., and Cuyler W. Brooks, J., "The NASA Langley Laminar-Flow-Control Experiment on a Swept, Supercritical Airfoil - Design Overview," NASA TP 2809, NASA Langley Research Center, May 1988.

[17]Harris, C. D. and Cuyler W. Brooks, J., "Modifications to the Langley 8-Foot Transonic Pressure Tunnel for the Laminar Flow Control Experiment," NASA TM 4032, NASA Langley Research Center, May 1988.

[18]http://gftd.larc.nasa.gov/facilities/ntf.html, "National Transonic Facility (NTF)," .

[19]Wahls, R. A., "The National Transonic Facility: A Research Retrospective (Invited)," AIAA Paper 2001-754, AIAA, January 2001.

[20]http://gftd.larc.nasa.gov/resources/NTF_User_Guide_2 26-13_small.pdf, "NTF User Guide," February 2012.

[21]Vassberg, J. C., DeHaan, M. A., Rivers, S. M., and Wahls, R. A., "Development of a Common Research Model for Applied CFD Validation Studies," AIAA Paper 2008-6919, AIAA, August 2008.

[22]Rivers, M. B. and Dittberner, A., "Experimental Investigation of the NASA Common Research Model (Invited)," AIAA Paper 2010-4218, AIAA, June 2010.

[23]Jacobs, P. F. and Gloss, B. B., "Longitudinal Aerodynamic Characteristics of a Subsonic, Energy-Efficient Transport Configuration in the National Transonic Facility," NASA TP 2922, NASA Langley Research Center, August 1989.

[24]Hemsch, M., Tuttle, D., Houlden, H., and Graham, A., "Measurement of Force Balance Repeatability and Reproducibility in the NTF," AIAA Paper 2004-0771, AIAA, January 2004.

[25]Hemsch, M. J., "Analysis of Flow Angularity Repeatability Tests in the NTF," AIAA Paper 2006-0518, AIAA, January 2006.

[26]Walker, E. L., "Statistical Calibration and Validation of a Homogeneous Ventilated Wall-Interference Correction Method for the National Transonic Facility," NASA TP 2005-213947, NASA Langley Research Center, December 2005.

[27]Paryz, R. W., "Upgrades at the NASA Langley Research Center National Transonic Facility," AIAA Paper 2012-0102, AIAA, January 2012.

[28]Cramer, C. J., Wright, J. D., Simmons, S. A., Bobbitt, L. E., and DeMoss, J. A., "A Description of the Development, Capabilities, and Operational Status of the Test SLATE Data Acquisition System at the National Transonic Facility," AIAA Paper 2015-, AIAA, January 2015.

[29]http://www.testslate.com, "Test SLATE : Software for Laboratory and Automated Test Environments," .

[30]Kilgore, W. A., Balakrishna, S., and Butler, D. H., "Reduction of Tunnel Dynamics at the National Transonic Facility (Invited)," AIAA Paper 2001-1162, AIAA, January 2001.